

A Computational Method Based on Augmented Lagrangians and Fast Fourier Transforms for Composites with High Contrast

J.C. Michel¹, H. Moulinec, P. Suquet

Abstract: An iterative numerical method based on Fast Fourier Transforms has been proposed by Moulinec and Suquet (1998) to investigate the effective properties of periodic composites. This iterative method is based on the exact expression of the Green function for a linear elastic, homogeneous reference material. When dealing with linear phases, the number of iterations required to reach convergence is proportional to the contrast between the phases properties, and convergence is therefore not ensured in the case of composites with infinite contrast (those containing voids or rigid inclusions or highly nonlinear materials). It is proposed in this study to overcome this difficulty by using an augmented Lagrangian method. The resulting saddle-point problem involves three steps. The first step consists of solving a linear elastic problem, using the Fourier Transform method. In the second step, a nonlinear problem is solved at each individual point in the volume element. The third step consists of updating the Lagrange multiplier. This method was applied successfully to composites with high or infinite contrast. The first case presented here is that of a linear elastic material containing voids. The second example is that of a two-phase composite with power-law constituents. The third example involves voided rigid-plastic materials.

keyword: computational method, augmented lagrangians, fast fourier transforms, nonlinear composites

1 Introduction

An iterative numerical method based on Fast Fourier Transforms was recently proposed by Moulinec and Suquet (1994), Moulinec and Suquet (1998) to investigate the effective properties of composites with complex microstructures as well as their local responses. This method makes direct use of digital images of the “real” microstructure of the composite. It is based on the exact expression of the Green function for a linear elastic, homogeneous material. In the case of linear elastic phases, the problem is reduced to an integral equation (Lippmann-Schwinger equation), which is solved iteratively. The rate of convergence of the method is directly related to the contrast between the phases. When dealing with linear phases, the number of iterations required to reach convergence varies linearly with the elastic contrast, *i.e.* roughly speaking with the

ratio between the elastic Young moduli of the phases. Convergence is therefore not ensured in the case of composites with infinite contrast (those including voids or rigid inclusions). The method has been successfully applied to linear elastic and elastic-plastic composites by Moulinec and Suquet (1998). It cannot however be straightforwardly extended to other nonlinear material behaviors, such as power-law stress/strain relations: with materials of this kind, the initial moduli are very large and in addition, the secant moduli are highly contrasted in zones undergoing very different deformations.

The aim of the present paper is to extend this method to composites containing voids and nonlinear elastic phases.

We propose an augmented Lagrangian method (section 2), which has proved to be an efficient means of dealing with other nonlinear problems (see Glowinski and Le Tallec, 1989). The resulting saddle-point problem involves three steps. The first step consists of solving a linear elastic problem in the case of a homogeneous material (reference material) with eigenstresses. This problem can be solved using the Fourier transform of the Green function for the reference material. In the second step, a nonlinear problem is solved locally, *i.e.* at each individual point in the volume element. The third step consists of updating the Lagrange multiplier and is also a local step.

This method is applied successfully in section 3 to composites with high or infinite contrast. The first case is that of a linear elastic material containing voids. The second example is that of a two-phase composite with power-law constituents. The third example concerns the flow surface of voided rigid-plastic materials.

The problem under consideration can be stated as follows. A representative volume element V of the composite is composed of various phases with strain-energy $w(\mathbf{x}, \boldsymbol{\varepsilon})$ so that the stress-strain relation at point \mathbf{x} can be written

$$\boldsymbol{\sigma}(\mathbf{x}) = \frac{\partial w}{\partial \boldsymbol{\varepsilon}}(\mathbf{x}, \boldsymbol{\varepsilon}), \quad (1)$$

where w is a convex function of $\boldsymbol{\varepsilon}$. Its dependence on \mathbf{x} denotes a material nonhomogeneity. Material constraints can be included in the definition of w . For instance, with incompressible materials, $w = +\infty$ when $\text{tr}(\boldsymbol{\varepsilon}) \neq 0$.

The volume element V is subjected to an average strain \mathbf{E} . Periodicity conditions are assumed on the boundary of V . To be more specific, the local strain field $\boldsymbol{\varepsilon}(\mathbf{u})$ is split into its average

¹ Corresponding author. Email: michel@lma.cnrs-mrs.fr. LMA/CNRS, 31 Chemin Joseph Aiguier, 13402 Marseille Cedex 20. France.

\mathbf{E} and a fluctuation term $\varepsilon(\mathbf{v})$:

$$\varepsilon(\mathbf{u}) = \mathbf{E} + \varepsilon(\mathbf{v}). \quad (2)$$

By assuming periodic boundary conditions, it is assumed that the fluctuating displacement \mathbf{v} is periodic (notation: $\mathbf{v} \#$), and that the traction $\boldsymbol{\sigma} \cdot \mathbf{n}$ is anti-periodic in order to meet the equilibrium equations on the boundary between two neighboring cells (notation: $\boldsymbol{\sigma} \cdot \mathbf{n} - \#$).

It is known (see, for example, Suquet, 1987; Ponte Castañeda and Suquet, 1998) that the effective behavior of the composite also results from an effective strain-energy W^{hom} , which can be characterized by the variational property:

$$W^{\text{hom}}(\mathbf{E}) = \min_{\mathbf{u} \in K(\mathbf{E})} \langle w(\varepsilon(\mathbf{u})) \rangle, \quad (3)$$

where $\langle \cdot \rangle$ denotes the spatial average over V , and

$$K(\mathbf{E}) = \{ \mathbf{u} \text{ such that } \varepsilon(\mathbf{u}) = \mathbf{E} + \varepsilon(\mathbf{v}), \mathbf{v} \# \}, \quad (4)$$

is the set of displacement fields which are kinematically admissible with the average strain \mathbf{E} .

2 Augmented Lagrangian method

2.1 General formulation

Problem (3) can be reformulated as a minimization problem under constraint

$$\text{Min}_{\mathbf{e}} \left\{ \text{Min}_{\mathbf{u} \in K(\mathbf{E})} \langle w(\mathbf{e}) \rangle \right\}, \quad (5)$$

under the constraint (compatibility condition)

$$\varepsilon(\mathbf{u}(\mathbf{x})) - \mathbf{e}(\mathbf{x}) = 0 \quad \forall \mathbf{x} \in V. \quad (6)$$

Let $\lambda(\mathbf{x})$ denote the Lagrange multiplier associated with this constraint, and consider the augmented Lagrangian

$$L_{\mathbf{c}_0}(\varepsilon(\mathbf{u}), \mathbf{e}, \lambda) = \langle w(\mathbf{e}) \rangle + \langle \lambda : (\varepsilon(\mathbf{u}) - \mathbf{e}) \rangle + \frac{1}{2} \langle (\varepsilon(\mathbf{u}) - \mathbf{e}) : \mathbf{c}_0 : (\varepsilon(\mathbf{u}) - \mathbf{e}) \rangle. \quad (7)$$

The fourth-order tensor \mathbf{c}_0 possesses the usual symmetries characteristic of a stiffness tensor. It is chosen depending on the problem under consideration.

Problem (5) with constraint now turns into a saddle-point problem for $L_{\mathbf{c}_0}$. The saddle-point can be reached by means of the following Uzawa's algorithm (Glowinski and Le Tallec, 1989; Licht and Suquet, 1986):

Iterate i : given \mathbf{e}^{i-1} and λ^{i-1} ,

(1) compute $\varepsilon(\mathbf{u}^i)$ solution of the problem:

$$\text{Min}_{\mathbf{u} \in K(\mathbf{E})} L_{\mathbf{c}_0}(\varepsilon(\mathbf{u}), \mathbf{e}^{i-1}, \lambda^{i-1}), \quad (8)$$

(2) compute \mathbf{e}^i solution of the nonlinear equation (at each point \mathbf{x}):

$$\frac{\partial w}{\partial \mathbf{e}}(\mathbf{x}, \mathbf{e}^i) + \mathbf{c}_0 : \mathbf{e}^i(\mathbf{x}) = \mathbf{c}_0 : \varepsilon(\mathbf{u}^i(\mathbf{x})) + \lambda^{i-1}(\mathbf{x}), \quad (9)$$

(3) update λ^i :

$$\lambda^i(\mathbf{x}) = \lambda^{i-1}(\mathbf{x}) + \mathbf{d}_0 : (\varepsilon(\mathbf{u}^i(\mathbf{x})) - \mathbf{e}^i(\mathbf{x})). \quad (10)$$

\mathbf{d}_0 is a fourth-order tensor which serves to give the descent direction in Uzawa's algorithm. As usual, once convergence has been reached, \mathbf{e} coincides with $\varepsilon(\mathbf{u})$ and λ is the stress $\partial w(\varepsilon(\mathbf{u}))/\partial \varepsilon$.

2.2 Step 1: auxiliary Problem (8)

Problem (8) is a classical elasticity problem for a homogeneous, linear elastic medium with stiffness moduli \mathbf{c}_0 . This homogeneous material will be referred to here as the reference medium. The Euler equations associated with (8) can be formulated in terms of the fluctuation \mathbf{v} associated with \mathbf{u}

$$\left. \begin{aligned} \boldsymbol{\sigma}(\mathbf{x}) &= \mathbf{c}_0 : \varepsilon(\mathbf{v}(\mathbf{x})) + \boldsymbol{\tau}(\mathbf{x}) \quad \forall \mathbf{x} \in V, \\ \text{div } \boldsymbol{\sigma}(\mathbf{x}) &= \mathbf{0} \quad \forall \mathbf{x} \in V, \quad \mathbf{v} \#, \boldsymbol{\sigma} \cdot \mathbf{n} - \# \end{aligned} \right\} \quad (11)$$

where the periodic polarization field $\boldsymbol{\tau}(\mathbf{x})$ reads

$$\boldsymbol{\tau}(\mathbf{x}) = \lambda^{i-1}(\mathbf{x}) - \mathbf{c}_0 : \mathbf{e}^{i-1}(\mathbf{x}) + \mathbf{c}_0 : \mathbf{E}. \quad (12)$$

Note that $\mathbf{c}_0 : \mathbf{E}$ is constant, and thus divergence-free, and can be dropped from the previous expression for the determination of \mathbf{v} . The solution of (11) can be expressed in real and Fourier spaces, respectively, by means of the periodic Green operator Γ^0 associated with the reference medium with elasticity tensor \mathbf{c}_0 . In real space

$$\varepsilon(\mathbf{v}(\mathbf{x})) = -\Gamma^0 * \boldsymbol{\tau}(\mathbf{x}) \quad \forall \mathbf{x} \in V, \quad (13)$$

or in Fourier space

$$\widehat{\varepsilon}(\boldsymbol{\xi}) = -\widehat{\Gamma}^0(\boldsymbol{\xi}) : \widehat{\boldsymbol{\tau}}(\boldsymbol{\xi}) \quad \forall \boldsymbol{\xi} \neq \mathbf{0}, \widehat{\varepsilon}(\mathbf{0}) = \mathbf{0}. \quad (14)$$

The Fourier transform of the operator Γ^0 can be explicitly determined by taking the Fourier transform of (11). For instance, when the stiffness tensor \mathbf{c}_0 is isotropic, in the form

$$(c_0)_{ijkl} = \lambda_0 \delta_{ij} \delta_{kl} + \mu_0 (\delta_{ik} \delta_{jl} + \delta_{jk} \delta_{il}), \quad (15)$$

$\widehat{\Gamma}^0$ takes the explicit form

$$\widehat{\Gamma}_{ijkh}^0(\xi) = \frac{1}{4\mu_0|\xi|^2} (\delta_{ki}\xi_h\xi_j + \delta_{hi}\xi_k\xi_j + \delta_{kj}\xi_h\xi_i + \delta_{hj}\xi_k\xi_i) - \frac{\lambda_0 + \mu_0}{(\lambda_0 + 2\mu_0)\mu_0} \frac{\xi_i\xi_j\xi_k\xi_h}{|\xi|^4}. \quad (16)$$

Note (with Suquet and Moulinec, 1997) that this operator has a well defined limit when $\lambda_0 \rightarrow +\infty$ (*i.e.* when the reference medium is incompressible), which reads:

$$\widehat{\Gamma}_{ijkh}^0(\xi) = \frac{1}{4\mu_0|\xi|^2} (\delta_{ki}\xi_h\xi_j + \delta_{hi}\xi_k\xi_j + \delta_{kj}\xi_h\xi_i + \delta_{hj}\xi_k\xi_i) - \frac{1}{\mu_0} \frac{\xi_i\xi_j\xi_k\xi_h}{|\xi|^4}. \quad (17)$$

The pressure field (Lagrange multiplier for the incompressibility constraint) is also known in Fourier space:

$$\widehat{p}(\xi) = \frac{\xi_k \widehat{\tau}_{kh}(\xi) \xi_h}{|\xi|^2}. \quad (18)$$

2.3 Step 2: nonlinear equation (9)

Equation (9) is a tensorial nonlinear equation. When w is convex, *i.e.* when the operator $\partial w / \partial \varepsilon$ is monotone, this equation admits a unique solution which can be reached using any classical method (Newton's method, substitution method, etc.). There exist however three particular cases which are worth noting.

The first particular case corresponds to a nonhomogeneous linear material with stiffness $\mathbf{c}(\mathbf{x})$. Here (9) reduces to a linear equation which can be solved explicitly

$$\mathbf{e}^i = \varepsilon(\mathbf{u}^i) + (\mathbf{c}_0 + \mathbf{c})^{-1} (\lambda^{i-1} - \mathbf{c} : \varepsilon(\mathbf{u}^i)). \quad (19)$$

The case of voided materials corresponds to $\mathbf{c} = 0$ in the void phase.

The second case is that of nonlinear composites where all the phases are incompressible. The composite itself is incompressible and the reference material is therefore taken to be incompressible, with shear modulus μ_0 . In addition, it is assumed that the strain–energy $w(\varepsilon)$ depends only on the von Mises strain. To be more specific, the mean part and the deviatoric part of a second-order tensor \mathbf{a} are defined as

$$a_m = \frac{1}{3} \text{tr}(\mathbf{a}), \quad \mathbf{a}^{\text{dev}} = \mathbf{a} - a_m \mathbf{i}. \quad (20)$$

The nonlinear phases are assumed to be isotropic with strain–energy

$$w(\varepsilon) = f(\varepsilon_{\text{eq}}) \text{ when } \varepsilon_m = 0, \quad w(\varepsilon) = +\infty \text{ when } \varepsilon_m \neq 0, \quad (21)$$

where $\varepsilon_{\text{eq}} = \sqrt{\frac{2}{3} \varepsilon_{ij}^{\text{dev}} \varepsilon_{ij}^{\text{dev}}}$. Then

$$\frac{\partial w}{\partial \varepsilon} = -p \mathbf{i} + \frac{2}{3} \frac{f'(\varepsilon_{\text{eq}})}{\varepsilon_{\text{eq}}} \varepsilon. \quad (22)$$

The nonlinear equation (9) then reduces to

$$\left(\frac{1}{3\mu_0} \frac{f'(e_{\text{eq}}^i)}{e_{\text{eq}}^i} + 1 \right) \mathbf{e}^i = \varepsilon(\mathbf{u}^i) + \frac{1}{2\mu_0} (\lambda^{i-1})^{\text{dev}}. \quad (23)$$

We deduce from (23) that \mathbf{e}^i is colinear to $\varepsilon(\mathbf{u}^i) + 1/2\mu_0(\lambda^{i-1})^{\text{dev}}$ and that

$$\frac{1}{3\mu_0} f'(e_{\text{eq}}^i) + e_{\text{eq}}^i = \left(\varepsilon(\mathbf{u}^i) + \frac{1}{2\mu_0} (\lambda^{i-1})^{\text{dev}} \right)_{\text{eq}}. \quad (24)$$

The tensorial nonlinear equation (9) reduces to the scalar nonlinear equation (24).

The third case of interest is that of compressible isotropic nonlinear materials with a strain–energy w which can be written

$$w(\varepsilon) = g(\varepsilon_m, \varepsilon_{\text{eq}}). \quad (25)$$

Then

$$\frac{\partial w}{\partial \varepsilon} = \frac{1}{3} \frac{\partial g}{\partial \varepsilon_m} \mathbf{i} + \frac{2}{3} \frac{1}{\varepsilon_{\text{eq}}} \frac{\partial g}{\partial \varepsilon_{\text{eq}}} \varepsilon^{\text{dev}}. \quad (26)$$

The nonlinear equation (9) then reduces to a system of coupled nonlinear scalar equations

$$\left. \begin{aligned} \frac{1}{3} \frac{\partial g}{\partial \varepsilon_m}(e_m^i, e_{\text{eq}}^i) + 3k_0 e_m^i &= 3k_0 \varepsilon_m(\mathbf{u}^i) + \lambda_m^{i-1}, \\ \frac{1}{3\mu_0} \frac{\partial g}{\partial \varepsilon_{\text{eq}}}(e_m^i, e_{\text{eq}}^i) + e_{\text{eq}}^i &= \left(\varepsilon^{\text{dev}}(\mathbf{u}^i) + \frac{1}{2\mu_0} (\lambda^{i-1})^{\text{dev}} \right)_{\text{eq}} \end{aligned} \right\} \quad (27)$$

where k_0 is the bulk modulus of the reference medium ($3k_0 = 3\lambda_0 + 2\mu_0$).

2.4 Step 3: updating the Lagrange multiplier (10)

Although several choices are possible for the fourth-order tensor \mathbf{d}_0 , we have implemented Uzawa's algorithm with $\mathbf{d}_0 = \mathbf{c}_0$. This simple choice has some advantages. In the particular case of voided materials (linear or nonlinear), it can be checked that it leads to $\lambda^i = 0$ in the voids. Equilibrium is then met in the voids at each iteration.

2.5 Algorithm

An iterate of the above Uzawa's algorithm typically reads :

$$\begin{aligned} \text{Iterate } i : & \text{ given } \mathbf{e}^{i-1} \text{ and } \lambda^{i-1}, \\ (a) & \tau^{i-1}(\mathbf{x}) = \lambda^{i-1}(\mathbf{x}) - \mathbf{c}_0 : \mathbf{e}^{i-1}(\mathbf{x}), \\ (b) & \widehat{\tau}^{i-1} = F(\tau^{i-1}), \\ (c) & \widehat{\varepsilon}^i(\xi) = -\widehat{\Gamma}^0 : \widehat{\tau}^{i-1}(\xi) \quad \forall \xi \neq \mathbf{0}, \quad \widehat{\varepsilon}^i(\mathbf{0}) = \mathbf{E}, \\ (d) & \varepsilon^i = F^{-1}(\widehat{\varepsilon}^i), \end{aligned}$$

- (e) Solve (9) for $\mathbf{e}^i(\mathbf{x})$,
 (f) $\lambda^i(\mathbf{x}) = \lambda^{i-1}(\mathbf{x}) + \mathbf{c}_0 : (\boldsymbol{\varepsilon}^i(\mathbf{x}) - \mathbf{e}^i(\mathbf{x}))$,
 (g) convergence test.

F and F^{-1} denote the Fourier transform and the inverse Fourier transform, respectively.

The convergence test focuses on the compatibility equations and the stress-strain relations. More specifically, let us define the following norm for a second-order tensor:

$$\|\mathbf{a}\| = \max_{\mathbf{x}} \sqrt{\mathbf{a}(\mathbf{x}) : \mathbf{a}(\mathbf{x})}. \quad (28)$$

The iterative procedure is stopped when

$$\max \left(\frac{\|\boldsymbol{\varepsilon}^i - \mathbf{e}^i\|}{\|\mathbf{E}\|}, \frac{\|\lambda^i - \frac{\partial w}{\partial \boldsymbol{\varepsilon}}(\boldsymbol{\varepsilon}^i)\|}{\|\langle \frac{\partial w}{\partial \boldsymbol{\varepsilon}}(\mathbf{E}) \rangle\|} \right) \leq \eta, \quad (29)$$

with, typically in our calculations, $\eta = 10^{-5}$.

2.6 Discretization

In order to proceed with the numerical computations, the unit cell is discretized into $N_1 \times N_2$ pixels in the case of two-dimensional problems, or $N_1 \times N_2 \times N_3$ voxels in that of three-dimensional problems. The Fourier transform is replaced by the discrete Fourier Transform, which can be computed using the Fast Fourier Transform (detailed comments on the implementation of this technique are given in Moulinec and Suquet, 1998). The unknowns \mathbf{u} and $\boldsymbol{\varepsilon}$ are sampled by taking their values at these discrete pixels or voxels. The spatial discretization of the image induces a corresponding spatial discretization for the frequency $\boldsymbol{\xi}$ in Fourier space. For reasons which are closely linked to the FFT algorithm, the spatial resolution (number of pixels or voxels in each direction) is taken to be a power of 2.

2.7 Choice of the reference medium

The rate of convergence of the method depends on the choice of the stiffness \mathbf{c}_0 . Since we are not aware of any theoretical procedure yielding the optimum value of this tensor, we perform numerical tests to determine this optimum value.

In order to minimize the number of tests to be performed, it is worth noting that the optimum \mathbf{c}_0 does not depend very strongly on the spatial resolution of the image, as shown in Fig. 1. These results were obtained with the following data. The problem is a two-dimensional one. The unit cell is a square containing a circular void with a volume fraction of 0.196. The matrix is isotropic and linear elastic with Young modulus E and Poisson coefficient $\nu = 0.25$. The reference medium is isotropic with elastic properties $E_0 = rE$, $\nu_0 = \nu$. The loading applied is in-plane shear. The number of iterations at convergence is shown in Fig. 1 as a function of r and

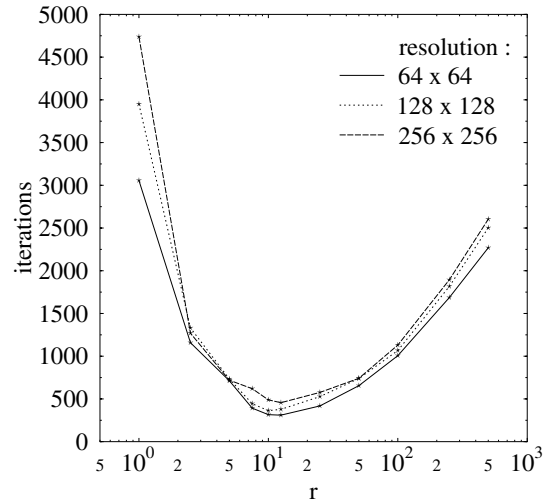


Figure 1 : Effects of the stiffness of the reference medium on the number of iterations to be performed at convergence with the augmented Lagrangian method.

of the image resolution (the number of pixels in the image). It can be seen that the method is highly sensitive to the choice of r but that it is relatively insensitive to the spatial resolution. The optimum value of r can therefore be determined at low resolutions and then used in computations at higher resolutions.

3 Examples

3.1 Voided linear materials

In this subsection, we discuss the case of a linear elastic matrix containing voids. The ratio between the Young's moduli of the phases is infinite, and this example can serve to check the ability of the method to deal with composites with infinite contrast. The cell is a cylinder with a square cross section and a width of $2a$. The void is a cylinder with a circular cross section and a radius R with $R/a = 16$ (void volume fraction $\simeq 3.10^{-3}$). The matrix material is isotropic with bulk and shear moduli k and μ respectively.

The volume element is subjected to an in-plane overall strain $\mathbf{E} = E_{\alpha\beta} \mathbf{e}_\alpha \otimes \mathbf{e}_\beta$, $\alpha, \beta = 1, 2$. The problem can be solved numerically within the framework of plane strains. Since the void volume fraction is small, the numerical solution can be compared with the exact result obtained for a void in an infinite matrix, which is known in the closed form. In the latter case, the deformation of the void in the infinite medium is homoge-

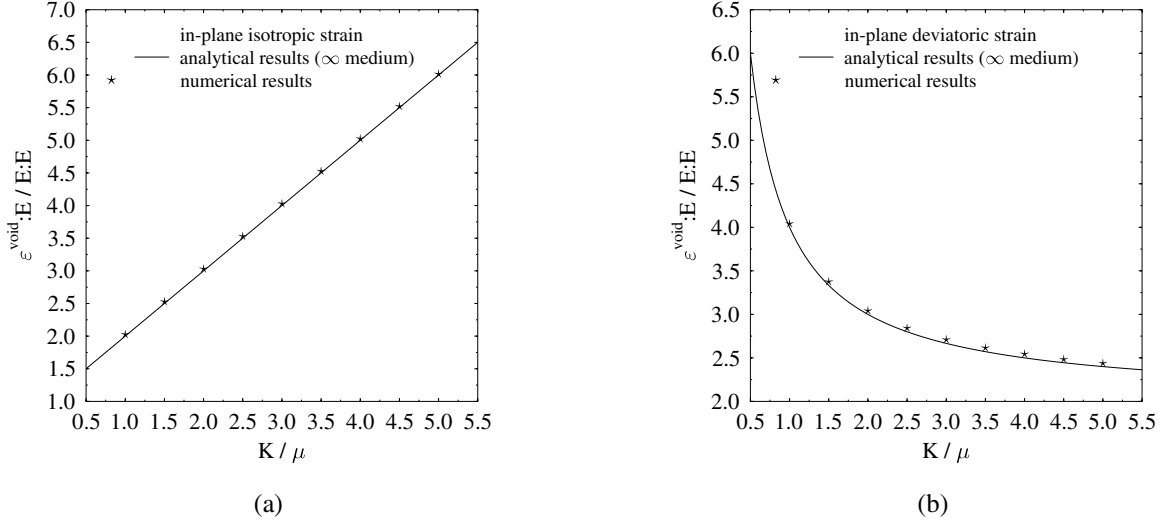


Figure 2 : Circular voids with a small volume fraction in a linear elastic material. Comparison between numerical and analytical results. (a): in-plane isotropic strain. (b): in-plane deviatoric strain.

neous and reads

$$\varepsilon_{\alpha\beta}^{\text{void}} = \frac{K+\mu}{\mu} \frac{E_{\gamma\gamma}}{2} \delta_{\alpha\beta} + 2 \frac{K+\mu}{K} \left(E_{\alpha\beta} - \frac{E_{\gamma\gamma}}{2} \delta_{\alpha\beta} \right), \quad (30)$$

where K is the in-plane bulk modulus ($K = k + (1/3)\mu$).

Two different types of loading were considered. The first one corresponds to in-plane compression ($E_{11} = E_{22} \neq 0$, other $E_{ij} = 0$). The second type of loading corresponds to in-plane shear ($E_{12} = E_{21} \neq 0$, other $E_{ij} = 0$). With each type of loading, the ratio K/μ was varied. The spatial resolution used in the numerical simulations was 1024×1024 pixels. The average deformations of the void obtained numerically and analytically are compared in Fig. 2. Keeping in mind that the numerical results were obtained with a small volume fraction (but not strictly 0), the agreement between the numerical results and the analytical ones can be said to be excellent.

3.2 Power-law materials

3.2.1 Constitutive relations

High-temperature creep in metals is commonly characterized by a power law relation between the strain-rate and the stress. Assuming incompressibility and isotropy and interpreting ε as the Eulerian strain-rate, the potential w of the material takes the form

$$w(\varepsilon) = \frac{\sigma_0 \varepsilon_0}{m+1} \left(\frac{\varepsilon_{\text{eq}}}{\varepsilon_0} \right)^{m+1} \quad \text{when } \varepsilon_m = 0, \\ w = +\infty \quad \text{when } \varepsilon_m \neq 0. \quad (31)$$

where ε_0 denotes a reference strain-rate, σ_0 is the flow stress and m is the rate-sensitivity exponent. Note that the strain-energy has the form (21). The constitutive relation is given

by

$$\sigma = -p \mathbf{i} + \sigma^{\text{dev}}, \quad \sigma^{\text{dev}} = \frac{\partial w}{\partial \varepsilon}(\varepsilon) = \frac{2\sigma_0}{3\varepsilon_0} \left(\frac{\varepsilon_{\text{eq}}}{\varepsilon_0} \right)^{m-1} \varepsilon, \quad (32)$$

where σ^{dev} is the stress deviator. Two particular cases of power-law materials can be mentioned. When $m = 1$, the material is linear incompressible with the shear (viscosity) modulus $\mu = \sigma_0/3\varepsilon_0$. When $m = 0$, the material is rigid-plastic with the flow stress σ_0 .

Computing the response of composites with power-law phases raises the same problems as those encountered with linear composites with high contrast. The local strain field is highly heterogeneous (the higher the nonlinearity, the more heterogeneous the strain field). Therefore the secant moduli defined as

$$\mu_{\text{sec}}(\varepsilon) = \frac{\sigma_0}{3\varepsilon_0} \left(\frac{\varepsilon_{\text{eq}}}{\varepsilon_0} \right)^{m-1}, \quad (33)$$

take values which can be very different. Nonlinear composites (even two-phase composites) behave like linear composites with infinitely many phases with highly contrasted secant moduli.

3.2.2 Cell materials

To illustrate the ability of the present method to overcome this difficulty, we consider the following class of two-phase composites, with a view to finding an accurate ‘‘self-consistent scheme’’ for nonlinear composites.

One of the basic issues which arises in the theoretical prediction of the effective properties of composite materials is to propose an appropriate description of the effective properties of

materials where there is no phase playing the role of a matrix. Polycrystalline materials are a typical example of such composites. Another example is provided by the duplex materials studied by Siegmund, Werner and Fischer (1993). These materials can be idealized as *cell materials*, to use Miller's terminology (Miller, 1969), in which the whole space is covered by cells. In the case of polycrystalline materials, the crystalline orientation of each cell is chosen randomly. In the case of duplex materials, the properties of each cell are chosen randomly to be either those of phase 1 or phase 2, subject only to the volume fraction constraints.

In the two-dimensional setting, when the materials are linear and incompressible, this problem has been studied from the computational point of view in particular by Suquet and Moulinec (1997). It was observed that when the contrast between the phases is not too large, the in-plane shear modulus of this class of composites can be accurately described by the self-consistent scheme. When the phases have equal volume fractions, the in-plane shear modulus of composites with interchangeable incompressible phases is given by the exact relation $\mu^{\text{hom}} = \sqrt{\mu^{(1)}\mu^{(2)}}$ (Helsing *et al.*, 1997), which coincides with the predictions of the self-consistent scheme.

The authors are not aware of the existence of any *exact* relations of this kind in the case of nonlinear materials, although rigorous nonlinear bounds and self-consistent estimates have been proposed during the past few years. This lack of exact results has motivated the present numerical study on the effective properties of nonlinear cell materials.

The microstructures investigated here are similar to those studied by Siegmund, Werner and Fischer (1993) and Suquet and Moulinec (1997). The problem is a two-dimensional one (all the phases are cylindrical in the third direction). The unit cell is a rectangle covered by hexagons which are identical in size (we used 16×16 hexagons). The flow stress σ_0 in each individual hexagon is prescribed randomly to be either that of phase 1 or phase 2, subject to only the volume fraction constraints. 25 different configurations were generated at the same volume fraction $c_1 = c_2 = 0.5$. These 25 configurations were converted into 50 by exchanging the two phases. Examples of these microstructures are shown in Fig. 3. Each microstructure is discretized into 1024×1024 pixels. The loading applied to the unit cells is a simple shear strain in the plane:

$$\mathbf{E} = \sqrt{3}\varepsilon_0 \mathbf{e}_1 \otimes_s \mathbf{e}_2. \quad (34)$$

The computations can be carried out in the framework of plane strains. The effective in-plane flow stress for each unit cell is computed as

$$\sigma_0^{\text{hom}} = \frac{\langle \boldsymbol{\sigma} : \boldsymbol{\varepsilon}(\mathbf{u}) \rangle}{\varepsilon_0}. \quad (35)$$

Numerical results are presented in Fig. 4a and Fig. 4b for two values of the contrast between the phases $\sigma_0^{(2)}/\sigma_0^{(1)} = 1.5$ and

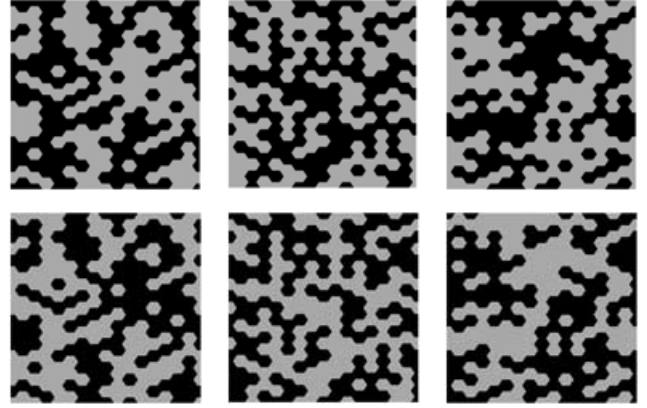


Figure 3 : Examples of microstructures. Both phases have equal volume fractions. The microstructures on the bottom row were deduced from those on the top by exchanging the phases.

5, and different values of the exponent m . The average values of the computed in-plane flow stresses for each exponent m are denoted by circles, while the scattering of numerical results about these mean values is indicated by error bars.

The numerical results were compared with various estimates and bounds available in the literature. The variational Reuss lower bound (VB(R)) is obtained by choosing a uniform stress field in the dual of the minimum principle (3). The result obtained for the effective in-plane flow stress is $\sigma_0^{\text{R}} \leq \sigma_0^{\text{hom}}$, with

$$\sigma_0^{\text{R}} = \left[\frac{c_1}{(\sigma_0^{(1)})^{\frac{1}{m}}} + \frac{c_2}{(\sigma_0^{(2)})^{\frac{1}{m}}} \right]^{-m}, \quad (36)$$

where the two phases are in the volume fractions c_1 and c_2 with flow stresses $\sigma_0^{(1)}$ and $\sigma_0^{(2)}$, respectively.

Variational procedures were recently developed (see Ponte Castañeda and Suquet, 1998, for a review) which improve on Reuss's nonlinear bound. Schematically, these procedures combine bounds or estimates for linear properties (those of a linear comparison solid) with a nonlinear variational scheme defining the appropriate linear comparison solid. When linear upper bounds are used in this procedure, rigorous upper bounds for the effective nonlinear properties of composites are obtained. For instance, the linear Hashin-Shtrikman upper bound (HS+) turns into a rigorous nonlinear upper bound for nonlinear composites (denoted VB(HS+)). Assuming that $\sigma_0^{(2)} \geq \sigma_0^{(1)}$, the variational HS-type upper bound VB(HS+) reads

$$\sigma_0^{\text{HS+}} = \sigma_0^{(1)} \min_{\rho > 0} f(\rho)^{\frac{m+1}{2}} \left[c_1 + c_2 \left(\frac{\sigma_0^{(2)}}{\sigma_0^{(1)}} \right)^{\frac{2}{1-m}} \rho^{\frac{m+1}{m-1}} \right]^{\frac{1-m}{2}} \quad (37)$$

with

$$f(\rho) = 1 + c_2 \frac{\rho - 1}{1 + c_1 \frac{\rho - 1}{\rho + 1}}. \quad (38)$$

Likewise, the self-consistent estimate VE(SC) can be derived from the variational procedure by estimating the effective properties of the linear comparison solid with the corresponding classical linear self-consistent scheme. However, when both phases have equal volume fractions, this nonlinear estimate reads (regardless of the nonlinearity exponent)

$$\sigma_0^{\text{hom}} = \sqrt{\sigma_0^{(1)} \sigma_0^{(2)}}. \quad (39)$$

Fig. 4 also shows the predictions of Michel's self-consistent scheme (Michel, 1998). In this scheme, one of the phases plays the role of a matrix while the other phase plays the role of inclusions. Let us assume for simplicity that phase 2 is harder than phase 1 (*i.e.* $\sigma_0^{(2)} \geq \sigma_0^{(1)}$). When phase 1 is the matrix (NSC(1)), the self-consistent estimate is given in an implicit form by the equation

$$\sigma_0^{\text{hom}} = (1 - c_2 a_2) \sigma_0^{(1)} \left[\frac{\sigma_0^{\text{hom}} - c_2 \sigma_0^{(2)} a_2^{m+1}}{c_1 \sigma_0^{(1)}} \right]^{\frac{m-1}{m+1}} + c_2 \sigma_0^{(2)} a_2^m, \quad (40)$$

with

$$\frac{\sigma_0^{(2)}}{\sigma_0^{\text{hom}}} a_2^m = \beta - (\beta - 1) a_2, \quad (41)$$

where β denotes the stress concentration factor under in-plane shear of a long rigid fiber in an infinite incompressible power-law matrix with potential W^{hom} in the form (31) with flow stress σ_0^{hom} . β depends on m but not on σ_0^{hom} . In the linear case ($m = 1$), β can be determined in the closed form: $\beta(1) = 2$. This is no longer the case when $m \neq 1$ and it is necessary here to perform a numerical computation for β . Some computed values of β for different exponents $n = 1/m$ are given in Tab. 1. When phase 2 is the matrix (NSC(2)), the implicit equation for the self-consistent estimate reads

$$\sigma_0^{\text{hom}} = (1 - c_1 a_1) \sigma_0^{(2)} \left[\frac{\sigma_0^{\text{hom}} - c_1 \sigma_0^{(1)} a_1^{m+1}}{c_2 \sigma_0^{(2)}} \right]^{\frac{m-1}{m+1}} + c_1 \sigma_0^{(1)} a_1^m, \quad (42)$$

with

$$\frac{\sigma_0^{(1)}}{\sigma_0^{\text{hom}}} a_1^m = \frac{\gamma - a_1}{\gamma - 1}, \quad (43)$$

where γ denotes the strain localization factor under in-plane shear of a long circular cylindrical void in an infinite incompressible power-law matrix with potential W^{hom} in the form

(31) with flow stress σ_0^{hom} . Again γ depends on m but not on σ_0^{hom} . Some computed values of γ for different exponents $n = 1/m$ are given in Tab. 1.

Table 1 : Michel's self-consistent scheme. Values of β and γ for different exponents $n = 1/m$.

n	1	1.5	2	3	5	7	10
β	2.	1.823	1.715	1.588	1.462	1.396	1.337
γ	2.	2.213	2.400	2.709	3.182	3.546	3.980

Finally, when the contrast is small (*i.e.* when $\sigma_0^{(2)}/\sigma_0^{(1)} = 1.5$), the numerical results can be compared with those obtained with the small-contrast expansion to second-order procedure developed by Ponte Castañeda and Suquet (1995).

Several comments can be made on these figures. First of all, it can be seen that all the numerical simulations and the various theoretical estimates satisfy the upper and lower variational bounds. With both contrasts, the numerical results obtained for σ_0^{hom} suggest that the effective flow stress is a non-decreasing function of m . As mentioned above, the variational self-consistent estimate VE(SC) does not predict that the nonlinearity exponent m will have any influence, and this is certainly a limitation of this prediction. With a small contrast ($\sigma_0^{(2)}/\sigma_0^{(1)} = 1.5$), the predictions of the small contrast expansion to second order and those of the two self-consistent estimates NSC(1) and NSC(2) are in good agreement with the numerical results. At a higher contrast ($\sigma_0^{(2)}/\sigma_0^{(1)} = 5$), the small contrast expansion is no longer valid and is not shown. The self-consistent estimates NSC(1) and NSC(2) diverge significantly when the nonlinearity increases. Finally NSC(2) seems to be the prediction which comes closest to numerical simulations for all values of m .

3.3 Rigid-plastic materials

3.3.1 Effective flow surface of a composite

Consider a composite where the individual constituents are rigid-plastic. The strength of the individual constituent located at point \mathbf{x} is characterized by a *strength domain* $P(\mathbf{x})$. P is a convex domain in the stress space which delimits the set of stress states which are physically sustainable by the material. The associated "energy" function w is defined as

$$w(\mathbf{x}, \boldsymbol{\varepsilon}) = \text{Sup}_{\boldsymbol{\tau} \in P(\mathbf{x})} \boldsymbol{\tau} : \boldsymbol{\varepsilon}. \quad (44)$$

w is a convex function whenever P is a convex set. For instance, when the strength properties of the phases are described by the von Mises criterion, this function reads

$$w(\mathbf{x}, \boldsymbol{\varepsilon}) = \sigma_0(\mathbf{x}) \varepsilon_{\text{eq}}. \quad (45)$$

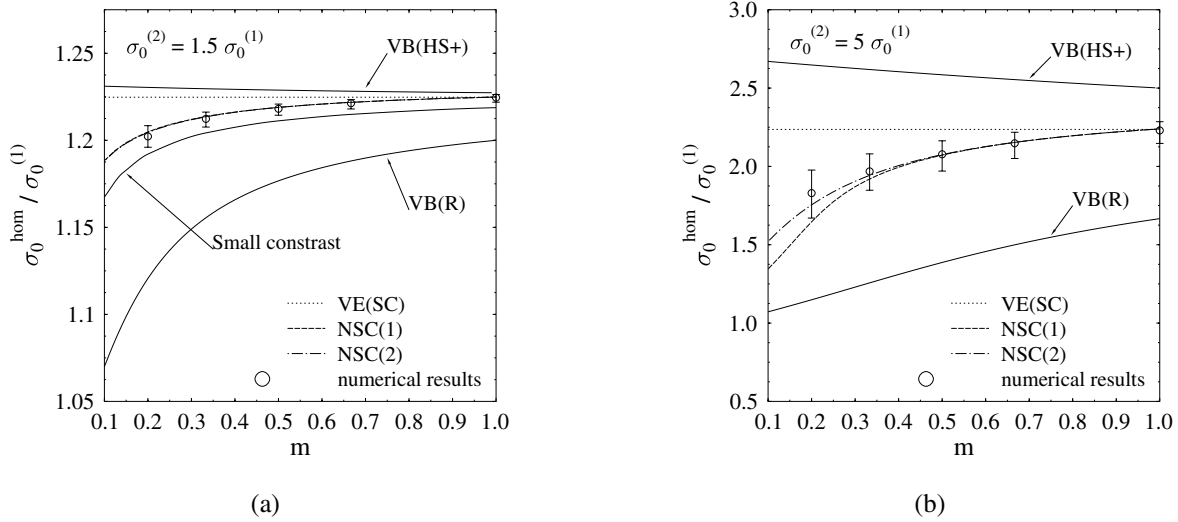


Figure 4 : Effective in-plane flow stress as a function of the power exponent m for two values of the contrast between the phases. Comparison between the theoretical predictions and the numerical simulations. VB(HS+): nonlinear Hashin-Shtrikman upper bound, VE(SC): variational self-consistent estimate, NSC(1): nonlinear self-consistent estimate (40)-(41), NSC(2): nonlinear self-consistent estimate (42)-(43), Small-contrast expansion Ponte Castañeda and Suquet (1995), VB(R): Reuss lower bound.

The *effective strength domain* of the composite has been defined as follows (Suquet, 1987)

$$P^{\text{hom}} = \left\{ \Sigma \text{ such that there exists } \sigma(\mathbf{x}) \text{ with } \langle \sigma \rangle = \Sigma, \right. \\ \left. \sigma(\mathbf{x}) \in P(\mathbf{x}), \operatorname{div} \sigma(\mathbf{x}) = \mathbf{0} \text{ for all } \mathbf{x} \text{ in } V, \right. \\ \left. \sigma \cdot \mathbf{n} = \# \right\}. \quad (46)$$

The boundary of P^{hom} is the *flow surface* of the composite. This surface depends on the strength domain, the volume fraction and the arrangement of the individual phases. The numerical determination of P^{hom} is difficult to perform based on the static definition (46), and a kinematic characterization is preferable. Let $W^{\text{hom}}(\cdot)$ denote the effective energy function associated with the individual energy $w(\mathbf{x}, \cdot)$ by the variational principle (3). It follows from Suquet (1987) that

$$W^{\text{hom}}(\mathbf{E}) = \operatorname{Sup}_{\Sigma \in P^{\text{hom}}} \Sigma : \mathbf{E} = \operatorname{Inf}_{\mathbf{u} \in K(\mathbf{E})} \langle w(\varepsilon(\mathbf{u})) \rangle. \quad (47)$$

The minimization problem (47) is non-smooth in the sense that the function w to be minimized is not differentiable at the origin. In the first step, the energy function is regularized by adding an elasticity term. This elasticity term is isotropic with bulk and shear moduli k and μ respectively. In the case of a von Mises material (45), the regularized energy reads

$$w(\mathbf{x}, \varepsilon) = \frac{9}{2} k \varepsilon_m^2 + f(\varepsilon_{\text{eq}}), \\ f(\varepsilon_{\text{eq}}) = \begin{cases} \frac{3}{2} \mu \varepsilon_{\text{eq}}^2 + \frac{\sigma_0^2}{6\mu} & \text{when } \varepsilon_{\text{eq}} \leq \frac{\sigma_0}{3\mu}, \\ \sigma_0 \varepsilon_{\text{eq}} & \text{when } \varepsilon_{\text{eq}} \geq \frac{\sigma_0}{3\mu}. \end{cases} \quad (48)$$

This strain-energy has the form (25).

We now consider the minimization problem (3) for the regularized energy (48), which is still denoted w . This problem is solved using a step-by-step procedure. The overall strain \mathbf{E} is applied gradually as

$$\mathbf{E}(t) = t \mathbf{E}_0, \quad (49)$$

where \mathbf{E}_0 is a prescribed direction of the strain. This introduces an artificial time into the problem. The evolution of the local fields $\sigma(t, \mathbf{x})$, $\mathbf{u}(t, \mathbf{x})$ solution of (3) is then computed. It can be seen that when t goes to infinity, the average stress $\Sigma(t) = \langle \sigma(t) \rangle$ stands on the flow surface ∂P^{hom} , and \mathbf{E}_0 is an outer normal vector to ∂P^{hom} at this point. The method can be modified to follow a prescribed direction in stress space $\Sigma(t) = k(t) \Sigma_0$, where Σ_0 is a given stress direction, instead of following direction in strain space as done by (49) (see Michel *et al.*, 1999, for further details along these lines). The latter stress-controlled method yields a more accurate determination of the extremal surface.

3.3.2 Voided rigid-plastic materials

We now consider the case of a rigid-plastic matrix containing voids. This problem involves two difficulties: the matrix is strongly nonlinear and the contrast between the phases is infinite. The problem is a two-dimensional one. The voids are infinite in the third direction and have a circular cross section and the same radius. The unit cell cross section is a square. 40 voids are distributed randomly in the unit cell (see Fig. 5a) and the resulting void volume fraction is $f = 0.125$. The unit

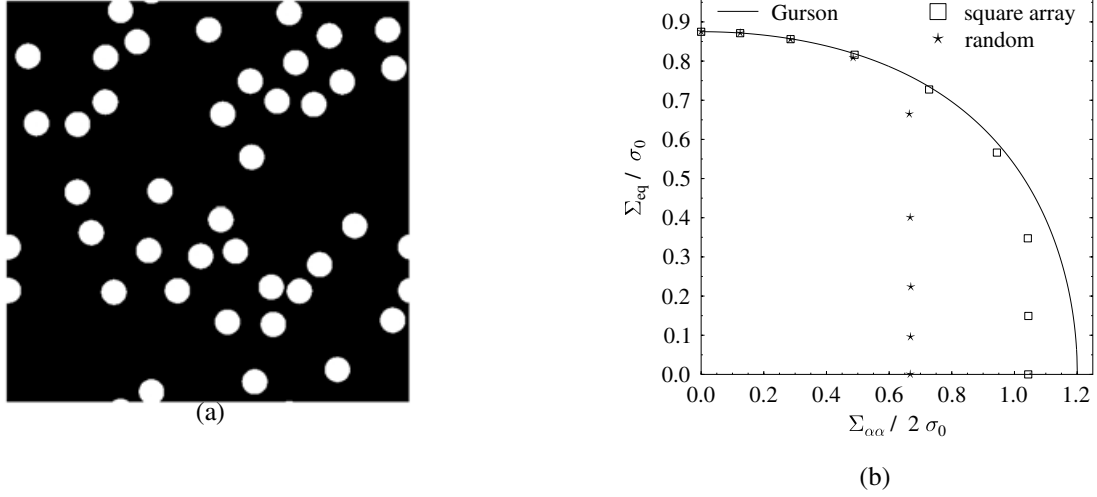


Figure 5 : Cylindrical voids randomly distributed in a block of plastic material. (a): configuration with 40 voids. (b): extremal surface under axisymmetric loading. Solid line: Gurson criterion for cylindrical voids. Squares: numerical results for a square void distribution. Stars: numerical results for the configuration with 40 randomly distributed voids.

cell cross section is discretized into 1024×1024 pixels. The overall stress is an axisymmetric one having the form

$$\Sigma = \Sigma_{11}(\mathbf{e}_1 \otimes \mathbf{e}_1 + \mathbf{e}_2 \otimes \mathbf{e}_2) + \Sigma_{33}\mathbf{e}_3 \otimes \mathbf{e}_3. \quad (50)$$

Three different results are shown and compared in Fig. 5b. The solid line is the Gurson criterion for cylindrical voids (Gurson, 1977):

$$\frac{\Sigma_{\text{eq}}^2}{\sigma_0^2} + 2f \cosh\left(\frac{\sqrt{3}\Sigma_{\alpha\alpha}}{2\sigma_0}\right) - 1 - f^2 = 0. \quad (51)$$

The squares denote the numerical results obtained with the present method on a simple unit cell consisting of a single circular void in a square cell with volume fraction $f = 0.125$. The stars denote the numerical results obtained on the unit cell shown in Fig. 5a. The results are plotted with $\Sigma_{\alpha\alpha}/2 = \Sigma_{11}$ on the horizontal axis and $\Sigma_{\text{eq}} = |\Sigma_{11} - \Sigma_{33}|$ on the vertical axis. The point on the vertical axis ($\Sigma_{11} = 0$ corresponding to uniaxial tension in the third direction) is known in the closed form $((1-f)\sigma_0)$, independently of the arrangement of the voids in the unit cell. The three sets of results deviate significantly when the triaxiality of the stress increases. The homogeneity (or nonhomogeneity) of the strain field within the unit cell strongly influences the extremal surface. Gurson's model, based on the analysis of a hollow cylinder, corresponds to a local strain field which is nonzero throughout, whereas the local field in the unit cell containing 40 voids is highly concentrated in the necks between the voids. This high strain concentration results in low strength properties. Finally the single void configuration comes in between these two extreme cases.

4 Conclusion

A numerical method based on Fast Fourier Transforms was recently proposed to compute the response of periodic composites (Moulinec and Suquet, 1998; Michel *et al.*, 1999). A major limitation of the original method is that convergence is slow in the case of composites with a high contrast and the method can even diverge when dealing with composites with infinite contrast (those containing voids or rigid inclusions or showing highly nonlinear behavior). In this paper, an augmented Lagrangian method is proposed which is free of these limitations. The method is successfully applied to the case of voided materials and power-law materials.

References

- Glowinski, R.; Le Tallec, P.** (1989): *Augmented Lagrangian and Operator-Splitting Methods in Nonlinear Mechanics*, vol. 9 of *Studies in Applied Mathematics*. SIAM.
- Gurson, A.** (1977): Continuum Theory of Ductile Rupture by Void Nucleation and Growth: Part I - Yield Criteria and Flow Rules for Porous Ductile Media. *J. Eng. Mat. Tech.*, vol. 99, pp. 1–15.
- Helsing, J.; Milton, G.; Movchan, A.** (1997): Duality relations, correspondences and numerical results for planar elastic composites. *J. Mech. Phys. Solids*, vol. 45, pp. 565–590.
- Licht, C.; Suquet, P.** (1986): Augmented Lagrangian method applied to a problem of incompressible viscoplasticity arising in homogenization. In: Taylor (ed) *Numerical Methods for Nonlinear Problems*, Pineridge Press, pp. 106–114.

Michel, J.C. (1998): A self-consistent estimate of the non-linear properties of isotropic two-phase composites. *Composites Science and Technology*, vol. 58, pp. 753–758.

Michel, J.C.; Moulinec, H.; Suquet, P. (1999): Effective properties of composite materials with periodic microstructure: a computational approach. *Comput. Methods Appl. Mech. Engrg.*, vol. 172, pp. 109–143.

Miller, M. (1969): Bounds for effective bulk modulus of heterogeneous materials. *J. Math. Phys.*, vol. 10, pp. 2005–2013.

Moulinec, H.; Suquet, P. (1994): A fast numerical method for computing the linear and nonlinear properties of composites. *C. R. Acad. Sc. Paris II*, vol. 318, pp. 1417–1423.

Moulinec, H.; Suquet, P. (1998): A numerical method for computing the overall response of nonlinear composites with complex microstructure. *Comput. Methods Appl. Mech. Engrg.*, vol. 157, pp. 69–94.

Ponte Castañeda, P.; Suquet, P. (1995): On the effective mechanical behavior of weakly inhomogeneous nonlinear materials. *Eur. J. Mech. A/Solids*, vol. 14, pp. 205–236.

Ponte Castañeda, P.; Suquet, P. (1998): Nonlinear composites. In: E. V. der Giessen and T. Wu (eds) *Advances in Applied Mechanics*, Academic Press, New York, vol. 34, pp. 171–302.

Siegmund, T.; Werner, E.; Fischer, F. (1993): Structure-property relations in duplex materials. *Comp. Mater. Sc.*, vol. 1, pp. 234–240.

Suquet, P. (1987): Elements of Homogenization for Inelastic Solid Mechanics. In: E. Sanchez-Palencia and A. Zaoui (eds) *Homogenization Techniques for Composite Media*, vol. 272 of *Lecture Notes in Physics*, Springer Verlag, pp. 193–278.

Suquet, P.; Moulinec, H. (1997): Numerical simulation of the effective properties of a class of cell materials. In: K. Golden, G. Grimmett, R. James, G. Milton and P. Sen (eds) *Mathematics of multiscale materials*, vol. 99 of *IMA Lecture Notes*, Springer-Verlag, New-York, pp. 277–287.